J. Phys.: Condens. Matter **11** (1999) 9365–9385. Printed in the UK PII: S0953-8984(99)05098-5

Growth of thin films

E Bauer

Department of Physics and Astronomy, Arizona State University, Tempe, AZ 85287-1504, USA

Received 10 June 1999

Abstract. The results of epitaxial growth studies of ferromagnetic metals for a selected class of nonmagnetic substrates is reviewed. The reverse sequence is also discussed for some systems of importance in double layer and sandwich studies. The interrelation between film structure and magnetic properties is pointed out for several examples.

1. Introduction

The rapid evolution of magnetic thin film sensors and memories during the past decade has not only led to an explosive growth of the literature on magnetic properties of thin films but to a similar development of studies of the growth of these films. This is in part due to the increasing number of experimental techniques suitable for growth studies and in part due to the recognition that the magnetic properties of the films depend strongly on the film structure which is largely determined by the growth. This article can, therefore, cover only a small fraction of the work in this field. It will not discuss the practical aspects of thin magnetic films. They can be found, for example, in the proceedings of the conferences on magnetic recording media [1] and of other conferences on magnetism and magnetic materials. Likewise, films on amorphous substrates, polycrystalline, sputtered and electrolytically deposited films will not be included. This leaves epitaxial layers grown under ultrahigh vacuum (UHV) conditions of which only a few could be selected. For a more general discussion of metal epitaxy on metals the reader is referred to older reviews [2, 3] and monographs, in particular to the articles in [4] which cover the various processes involved in epitaxy.

The review is organized as follows. After a brief description of the experimental methods growth on densely packed surfaces, mainly bcc (110) and fcc (111) surfaces will be discussed. Growth on fcc (100) surfaces is treated jointly with growth on bcc (100) surfaces. Films on other surfaces such as bcc (111), bcc (211), fcc (110) and hcp $(10\bar{1}0)$ as well as quasi-one-dimensional crystal growth on vicinal surfaces are touched only briefly. A discussion of the processes which allows us to tailor films such as nucleation control, use of misfit anisotropy, surfactants etc concludes this contribution.

2. Experimental methods

Of the many techniques in the arsenal of surface science the laterally averaging methods of reflection high energy electron diffraction (RHEED), low energy electron diffraction (LEED) and Auger electron spectroscopy (AES) have been most widely used in growth studies. Work function change ($\Delta\Phi$) measurements have also made valuable contributions, in particular in

0953-8984/99/489365+21$30.00

the monolayer range. More recently ultraviolet photoelectron spectroscopy (UPS) and x-ray photo-electron diffraction (XPD) have also been shown to be very useful. Although RHEED is still used for the determination of the film orientation, the specular beam intensity oscillations due to periodic atomic roughness changes has become its major application. Similarly, LEED not only gives the lateral periodicity and—with a dynamical intensity analysis—the atomic positions in the unit cell but in its SPALEED version—which has a high resolution in reciprocal space—also laterally averaged information on the surface topography. UPS allows us to monitor film growth via the sensitivity of the electronic structure to atomic environment up to several monolayers (ML) and XPD becomes an important tool for structural analysis beyond that thickness.

Our understanding of the growth of epitaxial films would be rudimentary were it not for the contributions which laterally resolving techniques, foremost scanning tunnelling microscopy (STM) and low energy electron microscopy (LEEM), have made. The initial problems of STM, thermal drift and shadowing by the tip, which made it impossible to monitor film growth, have been largely overcome so that growth processes can be studied now quasi-continuously by intermittent tip retraction. LEEM does not have these problems but at the expense of much lower lateral resolution than STM. However, many aspects of the growth do not need the resolution achievable with STM and the possibility to combine LEEM with LEED, spin-polarized LEEM (SPLEEM) and x-ray photo-emission electron microscopy (XPEEM) allows a comprehensive characterization of the topography, the crystal structure, the magnetic domain structure and the chemical composition of the film [5, 6]. The results reported below were obtained with a combination of several of these techniques. Others, of course, have contributed too but cannot be included here for lack of space.

3. Growth on densely packed surfaces

3.1. The bcc (110) surface

Although not close packed, these is the most densely packed surface of bcc metals and has long been a favourite substrate for epitaxy starting with the early studies of the growth of Cu on W(110) [7–9]. W(110) and Mo(110) substrates are so attractive because due to their high melting point they can be cleaned easily by flashing off deposited layers—with some precautions (see below)—so that they can be frequently reused. The (110) surfaces of the other bcc metals (Ta, Nb, Fe, Cr and V) are much harder to clean and have been used much less.

The surface energies of the ferromagnetic metals of interest here, Ni, Co and Fe are sufficiently lower than those of W and Mo so that Stranski–Krastanov growth is expected at elevated temperatures and quasi-Frank–van der Merwe growth at lower temperatures. On the basis of van der Merwe's structural phase diagram initially 1–2 pseudomorphic monolayers should form with the subsequent growth in the Nishiyama–Wassermann orientation of the fcc Ni and equivalent orientations of the hcp Co and the bcc Fe [10]. This growth sequence had already been observed earlier in the first AES/LEED/$\Delta\Phi$ study of Ni on W(110) [11] and was confirmed by the subsequent studies of this system [12–22] and of Ni on Mo(110) [23] with minor differences.

3.1.1. Ni on W(110) and Mo(110) The present state of understanding of the growth of Ni on W(110) and Mo(110) may be summarized as follows. At room temperature and below where nucleation rate is high and diffusion limited, two-dimensional (2D) pseudomorphic (ps) islands form initially with more or less dendritic shape. The 'dentricity' depends not only upon

deposition temperature and rate but also upon residual gas coadsorption, a problem encountered in all experiments in which the time between flashing the crystal and start of the deposition is long and/or the deposition is made cumulatively, for example in STM studies. Due to limited mobility, site blocking and possible Ehrlich–Schwoebel barriers at these temperatures, atoms landing on top of the islands cannot be incorporated at their edges and 'squeeze' into the island, transforming them into a close-packed (cp) structure with increasing coverage long before completion of the ps layer [24]. Alternatively the transition may occur spontaneously when two islands meet [11]. Only under very clean conditions and at elevated temperatures can the ps ML fully develop before the transition to the cp layer occurs. This is clearly evident in $\Delta\Phi$ measurements which are very sensitive to atomic roughness. Figure 1(a) shows in the upper part such $\Delta\Phi$ measurements for Ni on Mo(110) at temperatures at which kinetic limitations are negligible. Due to the loose packing in the ps ML Φ decreases initially nearly linear with coverage until the ps ML is completed and rises thereafter rapidly due to the formation of the cp layer. The subsequent change is slow because the 3D islands forming cover only a small fraction of the surface (600 K and 790 K) and because of alloying (880 K).

The AES measurements show only a small change of slope of the Ni signal at the ps $\rightarrow$ cp transition—which has been overlooked in less accurate work [13]—caused by changes in the electronic structure. These are clearly evident in the intensities of UPS spectra at energies which are particularly sensitive to structural changes as illustrated in figure 2 [17]. At a binding energy of 0.64 eV (b) the intensity suddenly increases strongly at the transition from ps to cp packing. For comparison also AES data are shown which were acquired at an emission angle (50°) more sensitive to structural changes than that used in figure 1(a) ($42 \pm 5^\circ$). Figure 2 also shows that the ps $\rightarrow$ cp transition occurs earlier at 300 K due to kinetic limitations. The effect of these limitations can be seen particularly well in figure 1(b) which shows the $\Delta\Phi$ change during heating after cumulative depositions of Ni on Mo(110) at 365 K. Above about $1/3$ ps ML heating causes initially an increase of Φ due to the incorporation of atoms on top of the ps islands and resulting ps $\rightarrow$ cp transition followed by a strong decrease to the equilibrium ps structure. The decrease is strongest around 1 ps ML as one would expect. The additional subtle features in these curves are explained in [23].

Recent STM studies [20–22] are in apparent contradiction with the picture of the ps $\rightarrow$ cp tranistion derived from the laterally averaging studies discussed above. In the STM studies the cp (7×1) structure at 0.9 ML coverage could not be converted into the ps structure by annealing at 900 K. Future work has to show whether this is due to the higher step density on the surface used in the STM study or due to contamination. The second possibility is not unlikely as LEEM studies of the initial growth of Co on W(110)—which is very similar to that of Ni—have also shown holes in the ML similar to those observed in the STM work whenever the surface was contaminated.

The growth beyond the first ML depends strongly upon temperature. At 300 K RHEED specular beam intensity oscillations can be seen over about 10 ML, depending upon the angle of incidence. Growth in poor vacuum increases the range of the oscillations significantly and so does deposition in good vacuum at 100 K [12, 15, 16]. This does not necessarily mean monolayer-by-monolayer growth as frequently assumed but indicates only that the surface roughness varies periodically during growth. Nevertheless, quasi-Frank–van der Merwe growth occurs at least initially as the Auger data up to three ML show. In recent LEED work the film strain along the W[$1\bar{1}0$] direction could be observed up to 8 ML before the surface became rough [25]. Although the temperature at which alloying sets in has not been determined accurately, there is little doubt on the basis of AES and energy loss spectroscopy that alloying between Ni and Mo starts definitely below 900 K and levels off at the approximate composition NiMo at about 1100 K in layers more than 4 ML thick [23]. The situation on W

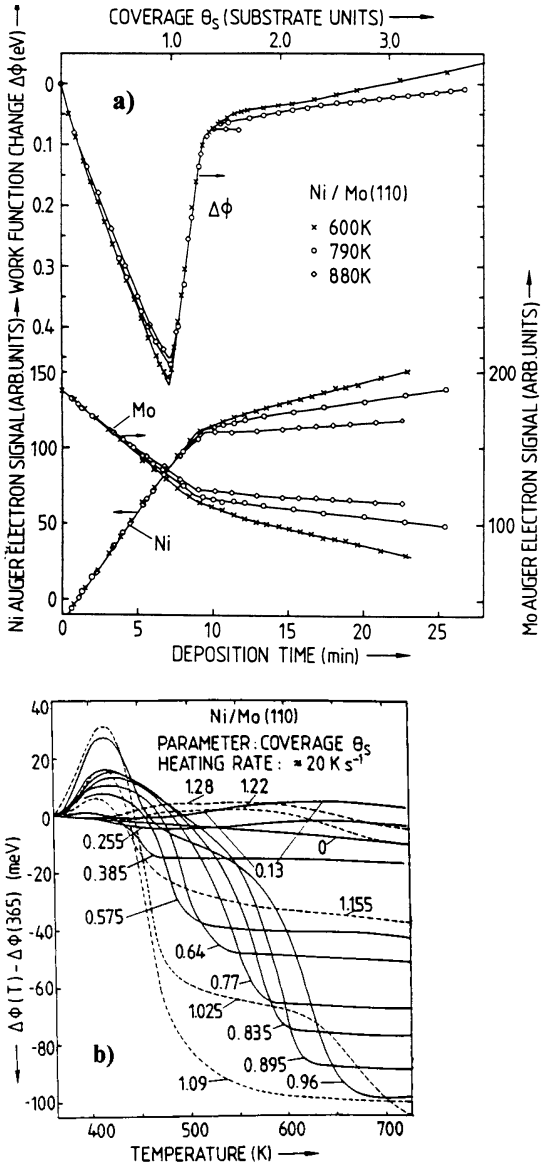

Figure 1. (a) Work function change $\Delta\Phi$, Ni and Mo Auger signals as a function of deposition time (bottom) and coverage (top) on Mo(110) at various temperatures, measured at temperature. (b) Work function change during heating after cumulative depositions at 365 K; coverage in ps units [23].

is believed to be similar [11]. It should be noted that the solubility of Ni in W and Mo is low but that W and Mo dissolve in Ni up to more than 20 at.%. Thus the Ni islands have to be large enough before alloying can start. No alloying occurs below 1 ML. The alloying problem is much clearer in Co films and will be discussed there in more detail. At lower temperatures the Ni layers grow in the Stranski–Krastanov mode as judged by the comparison with the AES and $\Delta\Phi$ data obtained at 300 K. For example, the slope of the AES signal in figure 1(a) beyond

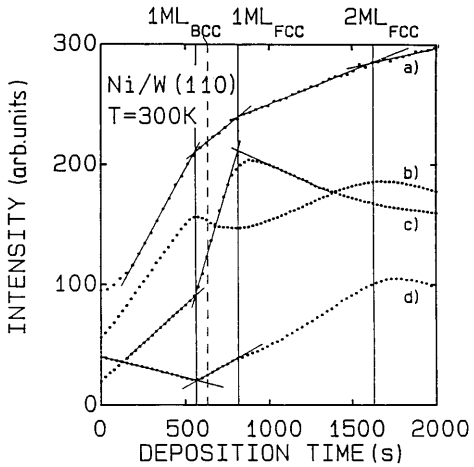

Figure 2. Ni AES and UPS signals as a function of deposition time (bottom) and coverage (top) on W(110). (a) Amplitude of differentiated $M_{2,3}M_{4,5}M_{4,5}$ (61 eV) Auger signal at a polar angle of 50° in the [001] azimuth. (b)–(d) UPS intensities in normal emission at 1.46 eV, 0.64 eV and 0.16 eV binding energy, respectively. The curves are shifted for clarity [17].

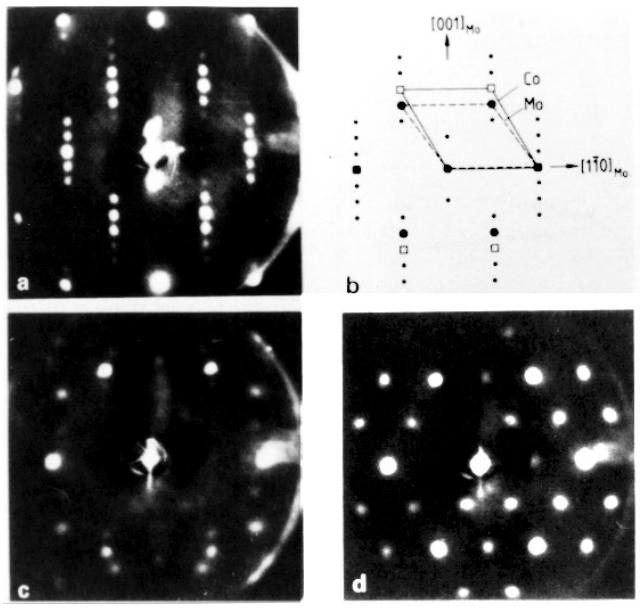

Figure 3. LEED patterns (a), (c), (d) and reciprocal lattice unit mesh (b) of pattern (a). (a), (b) (8×1), (b) complex and (c) $p(2 \times 2)$ structure. Energies 141 eV, 104 eV and 128 eV, respectively. (c) and (d) are from an alloy phase [23].

the first ML is significantly smaller at 600 K than at 300 K (not shown) and decreases further with increasing deposition temperature. More detailed data for Ni are not available.

3.1.2. Co on W(110) and Mo(110). The growth of Co on W(110) and Mo(110) has been studied in much more detail, though not with STM but with LEEM. First the results of the

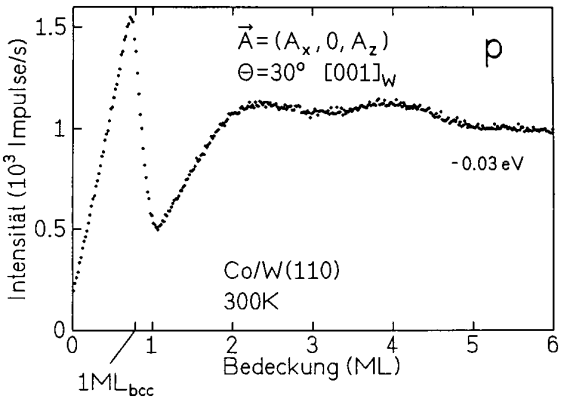

Figure 4. UPS intensity at a binding energy of 0.03 eV as a function of coverage measured during deposition at 300 K with parallel polarized light in the W [001] azimuth at a polar angle of 30° [27].

laterally averaging studies [23, 26–29] will be discussed. Co grows on both surfaces initially in the same manner as Ni does. Unless deposited or annealed at sufficiently high temperature the transition from the ps to the cp structure occurs as early as about 1/2 ML. The cp layer has the same characteristic (8 × 1) or (8 × 2) pattern—depending upon the definition of the substrate unit mesh—as the cp Ni layer (figure 3(a), (b)) [23]. Deposition at 750 K leads to very sharp changes in the structure-sensitive quantities such as AES, $\Delta\Phi$, UPS signals and LEEM contrast which allow a very accurate coverage and deposition rate calibration. However, even during room temperature deposition the ps → cp transition is usually clearly visible, for example in the UPS intensity versus coverage curve taken at a binding energy which is particularly sensitive to changes in the first monolayer (figure 4 [28]). The transition occurs here before the completion of the ps layer for reasons discussed above. The rounded transitions between the second and the third and the following monolayers shows that these layers are not completed before the start of the subsequent layer.

The growth of the first monolayer has been studied extensively by LEEM as a byproduct of SPLEEM [30] studies of thin Co films on W(110) for cleanness checks and deposition rate calibration. Figure 5 shows the influence of contamination on the step flow growth ((a),(b) [31]) and the transition from the ps to the cp monolayer ((c),(d) [32]). On a clean surface in good UHV the growth front is always smooth, at least at high temperatures. A rough growth front is a good indicator of contamination unless growth is crystallographically anisotropic, for example due to anisotropic strain. Anisotropic strain is responsible for the much higher growth rate of the cp layer in the [001] direction. This is seen in figures 5(c),(d) which show the monolayer shortly after the completion of the ps layer and before the completion of the cp layer. The layer is growing preferentially along the [001] direction because it is a 'floating layer' in this direction due to the large misfit while in the low misfit direction ([$1\bar{1}0$]) it is locked into the substrate.

Growth after completion of the monolayer is very similar to that of Ni. High resolution LEED measurements [29] indicate that the strain in the layer is constant up to about 9 ML and subsequently decreases inversely with thickness. AES [23], UPS and RHEED specular beam intensity oscillations [28] show that monolayer-by-monolayer growth rapidly deteriorates with increasing thickness at 300 K while at 100 K many RHEED oscillations can be seen. The layer is, however, less ordered at 100 K. LEEM studies have shown that films with minimum

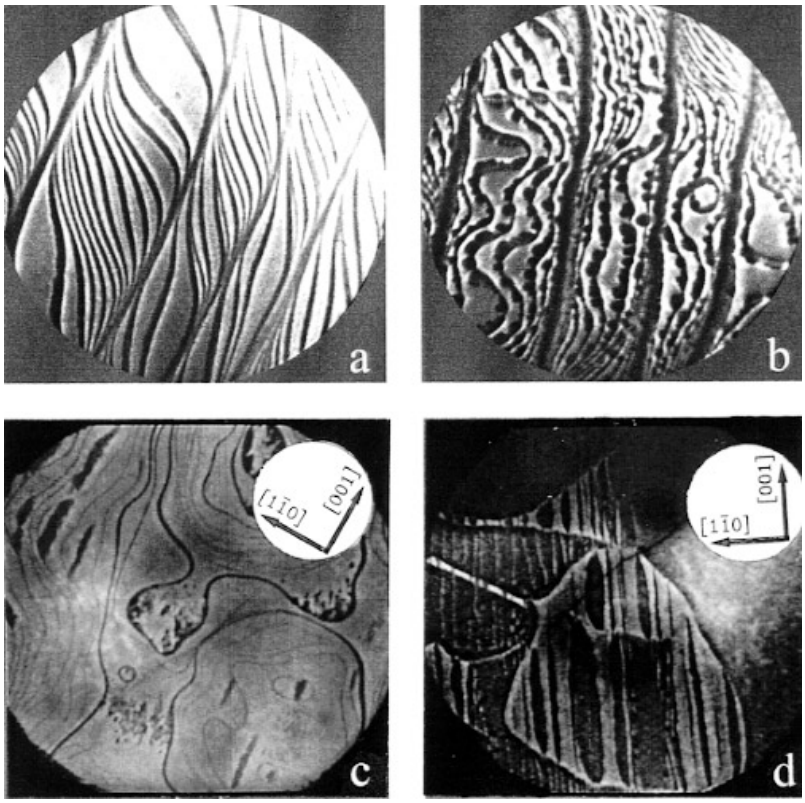

Figure 5. LEEM images of the early stages of the growth of the pseudomorphic Co layer on W(110) ((a), (b) [31]) and near the beginning and end of the close-packed monolayer ((c), (d) [32]) at 750 K. Field of view: 10, 8, 14 and 14 μm, electron energy 1.5, 1.5, 7 and 8.2 eV, in (a), (b), (c) and (d), respectively.

roughness, that is a three atomic layer level system, and good order can be obtained by depositing at temperatures just below the coalescence temperature. This increases diffusion on the existing film surface, reduces nucleation of the next monolayer on it and overcomes possible Ehrlich–Schwoebel barriers. The LEEM image of figure 6 [33] shows such a film surface at a mean thickness of about 5 ML. The film consists of regions which are 4, 5 and 6 ML thick.

Coalescence is very clearly evident in AES annealing experiments as illustrated in figure 7 [23]. The layer is stable up to about 450 K and then agglomerates strongly within a small temperature range. Above 750 K alloying starts, which leads to wetting and re-spreading of the Co alloy crystal over the surface. Annealing at 800 K is sufficient to produce the complex LEED pattern of figure 3(c). The AES extrema at about 850 K correspond to the composition Co_3Mo. Between 850 K and about 1150 K the alloy crystals agglomerate and at still higher temperatures Co sublimes from them leaving substrate mesa structures of the type seen in figure 8 [34] behind. If their formation is to be suppressed then desorption has to be done very fast so that the transport processes necessary for their formation cannot be effective. In thicker layers ($\geqslant$10 ML) coalescence is delayed and pre-empted by alloying which produces the p(2 $\times$ 2) pattern shown in figure 3(c).

Growth above 450 K is clearly of the Stranski–Krastonov type with a stable monolayer between the 3D crystals. This is illustrated in figure 8 [34] in which the mean film thickness

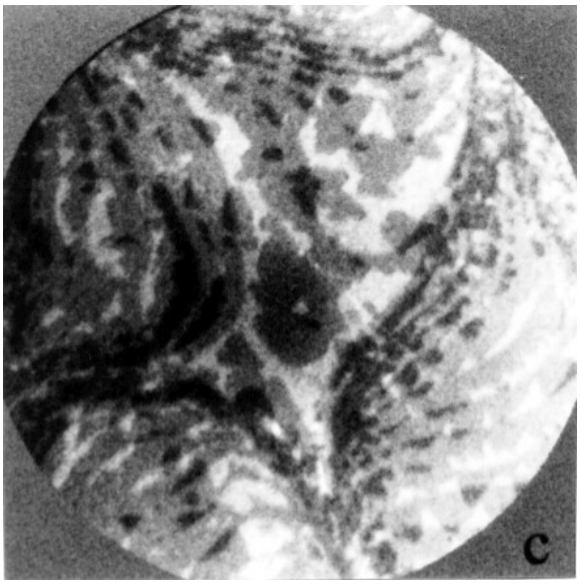

Figure 6. LEEM image of a 5 ML thick Co layer deposited on W(110) at about 400 K. Field of view 6 μm, electron energy 3 eV. Quantum size contrast [33].

increases from 4.5 ML to 11 ML. From the surface coverage by the 3D crystals the mean crystal thickness can be estimated to increase from 28 ML to 48 ML in the thickness range shown.

3.1.3. Fe on W(110) and Mo(110). Fe as the fundamental ferromagnetic metal has been studied most extensively with all methods listed at the beginning except LEEM, both on W(110) [35–46] and Mo(110) [23, 47]. In contrast to Ni and Co not only one ps ML grows at room temperature but also a metastable second one which is stable up to 650 K [37] or 770 K [46] on W(110) but only up to about 500 K on Mo(110) [23]. Thus there is no ps $\rightarrow$ cp transition in the first monolayer. Rather, ps islands grow up to about 0.6 ML at 300 K and then rapidly coalesce. The first 2D crystals of the second ML appear as early as 0.8 ML. Similarly, at higher coverages the next layer starts long before the preceding layer is completed [40, 42] which explains the pronounced rounding of the Auger signal–deposition time curves. In the first ML the islands grow rather isometrically, in the second ML preferentially along the W[001] direction. The preferential growth along this direction continues with further growth, leading to the 1D coarsening into roof-like facets along the [001] direction studied in detail on annealed Fe(110) films on W(110) [48]. This kinetic roughening phenomenon has also been used to grow corrugated Fe/Cr(110) superlattices whose morphology as a function of growth temperature and rate was studied in detail by RHEED and SEM [49].

At elevated temperatures growth occurs via step flow. The second ML is ps only up to about 1.2–1.3 ML [40] and then develops misfit dislocations along the [001] direction with an average spacing of about 4.6 nm. In the third layer the misfit in the W[1$\bar{1}$0] direction is still accommodated by dislocations along the W[001] direction but now with a more regular spacing of about 2.7 nm [40, 42]. Starting from the fourth ML onward the misfit in both substrate directions is accommodated by a 2D modulation of the lattice [40, 42–44] which had already been deduced earlier from LEED studies [35]. From 4 ML to about 10 ML, the thickest crystals

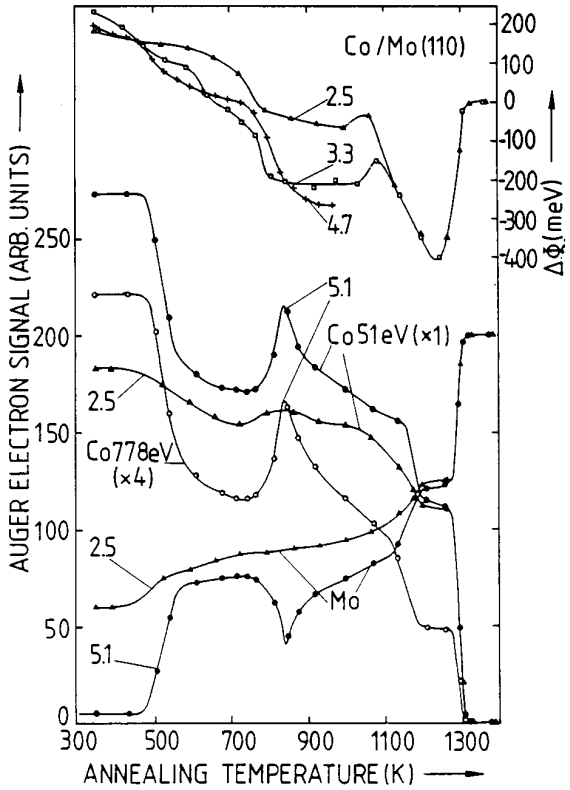

Figure 7. Co and Mo AES signals from 2.5 ML and 5.1 ML thick Co films on Mo(110) as a function of annealing temperature showing coalescence, alloying, coalescence and desorption [23].

on which this modulation can be seen in STM, the periodicity of the modulation corresponds to a complete strain relaxation of the Fe lattice and the crystals grow across substrate steps with flat top [40] faces similar to the Co crystals shown in figure 8. Coalescence, which starts in the intermediate thickness range (3–6 ML) already at about 600 K, begins in thicker films ($\geqslant$10 ML) above 750 K and is more or less completed at 850 K [46], resulting in large fully relaxed thick crystals surrounded by 1 ps ML [44, 46]. As already mentioned, the growth of Fe on Mo(110), which has been studied in considerable detail by AES, LEED, $\Delta\Phi$ and TDS measurements [23] and more recently by STM [47], is very similar to that on W(110). The details can be found in the original literature. Additional recent data of the growth of Fe on W(110) may be found in [50] (RHEED, AES) and [51] and [52] (stress, STM).

3.2. The hcp (0001) surface

Much less work has been done on these surfaces than on the bcc (110) surface. The growth of Ni on Re(0001) was studied by AES and LEED with the result that growth at 325 K occurs in the quasi-Frank–van der Merwe mode at least up to 4 ML and that the first ML is pseudomorphic. The subsequent MLs up to about 10 ML form an approximate (10×10) coincidence lattice which can be interpreted by a misfit dislocation network and double scattering [53]. These laterally averaged results are nicely confirmed by a more recent STM study [54]. Annealing above 600 K leads to coalescence [53]. The growth of Ni on Ru(0001) differs somewhat

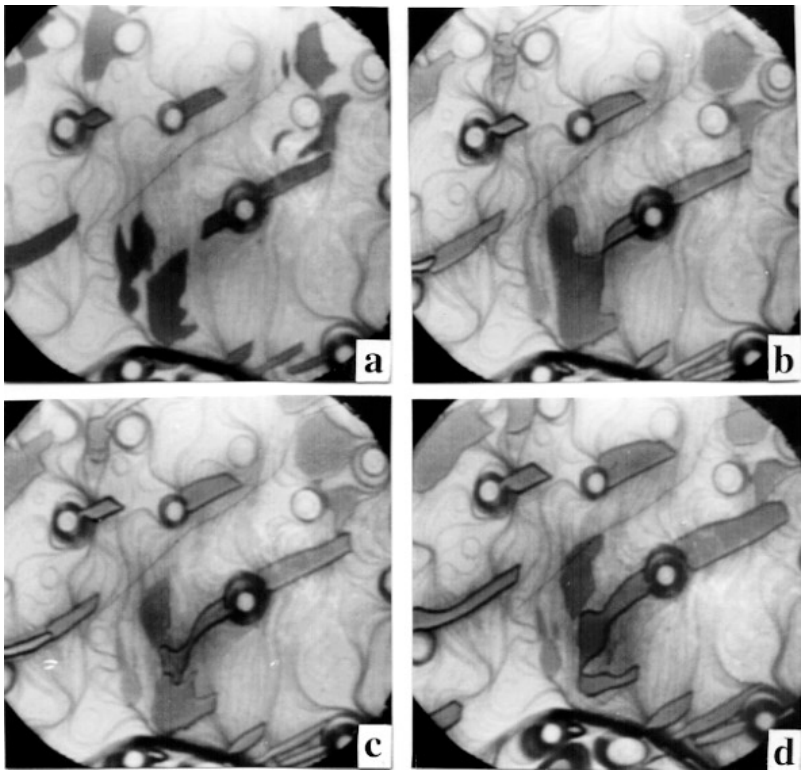

Figure 8. LEEM images selected from a series during deposition of Co on W(110) just below the onset of alloying. The Co crystals nucleate preferentially on the W mesas formed in many preceding Co desorptions and grow preferentially in the W[001] direction without noticeable impediment by substrate steps and step bunches. Accompanying SPLEEM images in the original work show that this is also the easy magnetization axis and that the crystals are single domains and maintain their magnetization also upon coalescence. The local magnetization is also maintained when a continuous film breaks up into islands with increasing annealing temperature [33].

from that on Re(0001) [55, 56]. A superstructure LEED pattern whose spot positions agree within the limits of error with those of an unstrained Ni(111) plane appears already above 0.5 ML. Annealing layers with this pattern leads to a (1×1) LEED pattern and reduces the work function considerably. This shows that the ps $\rightarrow$ cp transition occurs already in the first ML similar to the growth on the bcc (110) surfaces. The further growth is very much like that on Re(0001). Annealing leads to agglomeration of all material in excess of 1 ps ML. The agglomeration temperature increases with thickness from about 600 K at 2–3 ML to more than 1000 K at 5 ML.

The growth of Fe on Ru(0001) has been studied by several groups [56–60]. Quasi-Frank–van der Merwe growth is observed at 300 K initially. After the completion of the third ML AES suggests double layer growth. The first ML is pseudomorphic, the second and third show the LEED pattern of a transition structure to the unstrained Fe(110) orientation in three equivalent azimuthal orientations (Fe$[1\bar{1}1] \parallel$ Ru$[10\bar{1}0]$) which becomes clearer with increasing thickness and slight annealing. The agglomeration temperatures are strongly coverage dependent: about 400 K up to 4 ML, 520 K at 8 ML and 660 K at 12 ML. Between 760 K and 780 K alloying sets in which produces above 4 ML a LEED pattern attributed to the phase FeRu. The intensity

of this pattern decreases with increasing annealing temperature, accompanied by a decrease of the Fe Auger signal but a nearly constant Ru signal. This suggests thickening rather than agglomeration of the alloy. At coverages less than 4 ML only a (1×1) pattern is seen above 800 K [56].

Before concluding this section a few growth studies of nonmagnetic films on ferromagnetic films should be mentioned which are of relevance for the understanding of the influence of overlayers on magnetic properties and for the understanding of interlayer coupling between two magnetic layers and in superlattices. Examples are Cr on Co(0001) [61], Cu on Co(0001) [62] and Pt on Co(0001) [63].

3.3. The fcc (111) surface

The literature of the growth of ferromagnetic metals on fcc (111) surfaces is extensive so that only a few examples can be discussed which illustrate the complexity of the film growth when the surface energy of the layer material is larger than that of the substrate.

3.3.1. Au(111). Because of its $22 \times \sqrt{3}$ herringbone reconstruction this surface shows not only the complexities of the thermodynamically driven place exchange between film and substrate material but also those caused by the preferred nucleation at the point dislocations of the reconstruction. The very low coverage range, in which the preferred nucleation is best visible, has been studied extensively with STM, mainly in Co films [64–68] but also in Ni films [69–71] and Fe films [72]. Additional information for thicker films comes from AES [73, 74], helium-atom scattering [74], XPS [75] and magnetic measurements [68]. The three film/substrate systems have many things in common but differ also in some in part surprising aspects. Common features are (i) the preferred nucleation on the point dislocations at the herringbone corners on well ordered surfaces, (ii) the disappearance of the Auger signals above about 600 K in Ni and Co layers, probably also in Fe layers, and (iii) the approximate monolayer-by-monolayer growth from about 2 to 4 ML followed by increasingly rougher growth.

Differences exist in the manner in which the film crystals sink into the substrate and in how Au covers them with increasing temperature. The most striking difference is that the crystals formed initially are 1 ML thick in the case of Ni and Fe, but 2 ML thick in Co films, although the atomic diameters and surface energies (according to [76]) of the three materials differ very little. The references quoted reveal a great complexity of the place exchange between film and substrate material which depends strongly on material, coverage, deposition and annealing temperature and time. In any case, at temperatures above 400 K–450 K some Au has to be expected on top of the film material which is known to have a strong influence on the perpendicular anisotropy of the films, and at still higher temperatures very thin layers may be completely covered by Au. This restricts film growth on Au to considerably lower temperatures than on the refractory metals discussed in section 3.1.

3.3.2. Cu(111). Ferromagnetic films on Cu(111) have a long and conflicting history [77]. The article by Heinz in this issue describes the structure of the system Co/Cu(111) in detail so that only some of the apparent discrepancies between the various growth studies will be discussed briefly. They are to a large extent due to different growth and substrate conditions but in part also caused by the limitations of the methods used to characterize the growth via the structure of the resulting film. Growth was characterized by RHEED [77, 78], LEED, AES, STM, XPD, ion scattering spectroscopy, secondary electron angular distribution measurements, helium atom scattering and other techniques. For references see the article by Heinz and some of the recent work on this subject [79–85]. In agreement with theoretical expectations [86] initially crystals

form which are 2–3 ML high, one ML of which is sometimes at the level of the surrounding substrate surface. However, there are also other data [87] which appear incompatible with double layer growth and rather suggest monolayer-by-monolayer growth.

Cu moves easily onto the surface of these crystals, even at room temperature and rapidly around 400 K, covering the surface with a (sub)monolayer of Cu. Completion of the double layer depends strongly upon substrate temperature and deposition rate and occurs between 2 and 4 ML. The layers are pseudomorphic up to 6–7 ML according to some reports but the fcc $\rightarrow$ hcp transition in Co films occurs earlier. In Fe films the transition from fcc to bcc structure with Kurdyumov–Sachs starts as early as 2–3 ML in slow depositions while pulsed laser deposition which produces a much larger nucleation rate stabilizes the fcc structure up to about 6 ML [124, 125]. After the transition to the equilibrium crystal structure the films develop rapidly considerable roughness but Cu usually does not segregate to the surface of thick films unless they are annealed or deposited at elevated temperatures (400–500 K).

3.3.3. Other related work. There are numerous other studies on fcc (111) surfaces, mostly in connection with magnetic measurements but not detailed enough to give a clear picture of the film growth. On substrates with low surface energy such as Ag and Al phenomena similar to those discussed in 3.3.2 should occur while on substrates with high surface energy such as Rh, Pt or Ir only the heat of mixing which can be quite large in some combinations can drive interdiffusion during film growth or annealing.

The understanding of the reverse film growth, that is of nonmagnetic films on magnetic substrates, is also very important in connection with the influence of overlayers and of interlayer coupling as already mentioned. Cu has attracted most attention because of the long controversy over the conditions necessary for optimum antiferromagnetic coupling but Au has also been studied extensively. In the case of Cu STM [62] and LEEM [88] show in qualitative agreement that initially a monolayer forms but the second layer starts to grow before the completion of the first. Upon deposition at slightly elevated temperatures (e.g. 365 K) the second layer islands could be identified to be 2 ML thick [88]. Growth at elevated temperature (400 K) shows clear Stranski–Krastanov growth of Cu with one ps ML [89], causing a very rough interface for a subsequent Co film. Therefore, high deposition rates and/or low temperatures are necessary for the growth of sandwiches and superlattices with flat interfaces.

Although Au has a lower surface energy than Co the large misfit precludes initial monolayer formation [86]. During room temperature deposition on a Co film a smoothing of its surface was reported but by the time that 2 ML have been deposited the Au layer is already so rough that it produces a transmission RHEED pattern. Deposition at elevated temperatures, e.g. at 400 K, produces from the very beginning a surface which is so rough that it does not show the peak in the perpendicular anisotropy observed at 1 ML during room temperature deposition [88]. With increasing thickness the roughness increases to such an extent that roughness-induced biquadratic coupling becomes as strong as bilinear coupling in Co/Au/Co sandwiches [31].

4. Growth on (100) surfaces

4.1. The bcc (100) surface

In contrast to the fcc (100) surface the bcc (100) surface is not densely packed. The surface has a strong potential corrugation and, therefore, influences the growth of thin films to a much larger extent than the surfaces discussed up to now. This is, in particular, true for refractory metals because of their strong interaction with the film. Although being an equilibrium surface, the bcc (100) surface tends to reconstruct, a tendency which is enhanced by adsorption. For

example, it is now well established that the c(2×2) reconstruction observed upon annealing of $1/2$ ML of many metals is caused by formation of an ordered 2D surface alloy. Although there are many studies of the growth of nonmagnetic metals on W(100) and a few on Mo(100), Nb(100) and Ta(100) not much information is available about the growth of ferromagnetic metals beyond 2 ML.

Fe forms on W(100) initially 2 ps ML, followed by quasi-Frank–van der Merwe growth at room temperature and Stranski–Krastanov growth at elevated temperatures [38, 90–92]. The double layer is pseudomorphic and stable up to about 1100 K; thicker layers agglomerate above 500 K. A 4.4 ML thick film produces a diffuse, high background pattern which changes into a streaked pattern, followed by the (1×1) pattern of the ps double layer above 900 K. Fe fulfills the necessary criteria which favour the hcp structure beyond the initial ps layer (see below) but whether or not these are sufficient has to be decided by future work.

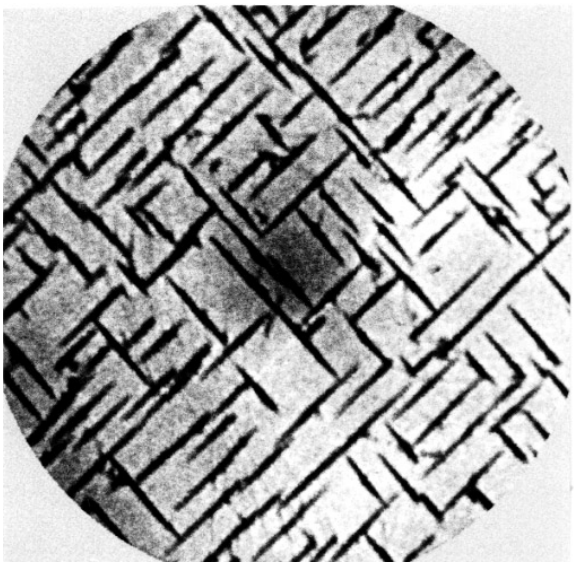

Figure 9. LEEM image of a 4 ML thick Co film grown on W(100) at 400 K. Field of view 9 μm, electron energy 8.3 eV [97].

In the case of Co [93–97] there is no doubt about the growth of hcp crystals after the completion of the ps double layer. Growth of the first ML produces negligible contrast in LEEM but the second ML shows pronounced step flow growth together with nucleation on larger terraces already at 400 K, at 500 K nearly only step flow growth. When deposited at lower temperatures and to larger thickness the hcp films are stable up to 400 K where already strong coalescence into the large hcp crystals with the orientation relationship Co($11\bar{2}0$) [$1\bar{1}00$] $\|$ W(100) [011], [$01\bar{1}$] occurs. They have a strongly elongated shape caused by the anisotropic misfit (figure 9 [96, 97]) which is already present during growth at temperatures as low as 150 K as seen by RHEED [95]. Above 700 K the crystals start to alloy with the substrate, probably by solution of W in Co at the positions at which the needle-like crystals cross substrate steps [97]. For Co and Ni on Mo(100) no detailed growth studies have been made with surface-sensitive techniques.

For Ni on W(100) information is available only on the initial growth [98, 99] but there is little doubt on the basis of misfit considerations that the layer should grow in the hcp structure with ($11\bar{2}0$) orientation after the initial pseudomorphic layer.

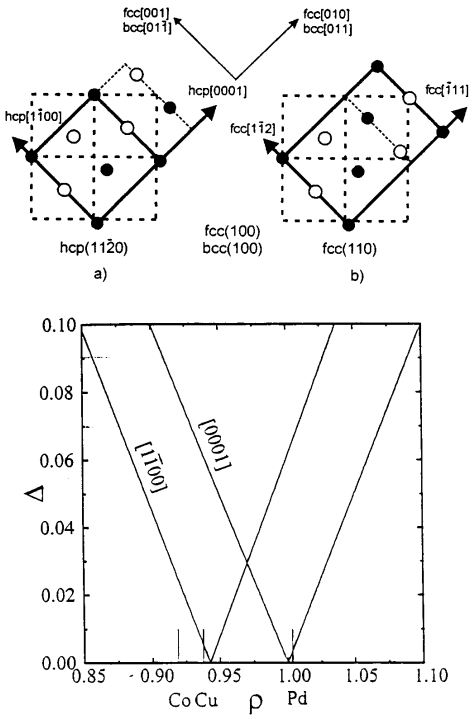

Figure 10. Orientation relationships of (a) hcp (11$\bar{2}$0) and (b) fcc (110) planes on bcc and fcc (100) surfaces (heavy dashed lines) and misfit Δ along the [1$\bar{1}$00] and [0001] directions as a function of the ratio ρ of the atomic radii of film and substrate atoms. Some ρ values for W are indicated. Full and open circles in (a), (b) first and second atomic layer, respectively [104, 106].

Concluding this section some STM work on Fe(100) should be mentioned. It concerns the growth of Fe and Cr on this surface. The Fe study establishes the connection between RHEED specular beam intensity oscillations and the microstructure [100]; the growth of Cr on Fe(100) is important for the understanding of the deposition temperature dependence of the interlayer coupling between Fe films through Cr spacers [101, 102].

4.2. The fcc (100) surface

Ferromagnetic films on these surfaces are dealt with in more detail in Heinz's article, in particular the ferromagnetic very rich Fe/Cu(100) system and the Ni/Cu(100) system. The growth of Co on Cu(100) and of the three ferromagnetic metals on Ag, Au and Al surfaces has also been studied somewhat. All of these systems are prone to the same intermixing problem mentioned above in connection with the corresponding (111) surfaces which to a large extent is specific for each system, the surface and the deposition conditions so that generalizations are difficult. One common feature is that in many cases pseudomorphic growth occurs over several monolayers before the film converts into its usual crystal structure.

In many film/substrate combinations, however, epitaxial strain is large enough to induce growth in a non-equilibrium structure. This is due to the fact that the structural modifications of many metals differ but little in total energy so that the additional strain energy induced by the misfit can tilt the energy balance to a non-equilibrium structure. Examples are the bct and fct structure in various systems but a more dramatic one is the formation of an hcp layer after

the initial pseudomorphic layer. This can occur for a certain range of the ratio $\rho = d_F/d_S$ of the atomic radii of film and substrate atoms in which the misfit Δ along the [0001] and [$1\bar{1}00$] directions of the hexagonal modification of the film material is small in the orientation shown in figure 10(a) [103–105]. In the bottom of this figure Δ is plotted as a function of ρ. From $\rho = 0.90$ to $\rho = 1.07$ the maximum misfit in one direction is 10% while in the other direction it is significantly smaller. The ρ values for some layers which grow in hcp structure on W(100) are indicated at the bottom. Figure 10(b) shows the competing fcc orientation in which the (110) plane is parallel to the substrate. The stacking sequence ABC of the close-packed planes has a much less favourable interface than that of the hcp layer, AB. As a consequence fcc films can grow in the hcp structure to considerable thickness before they transform into the fcc (110) orientation observed in thick films a long time ago [106].

The hcp ($11\bar{2}0$) $\parallel$ bcc (100) orientation relationship is well established for Co on Cr [107, 108], FeAl [109] and W [95] and more recently also for an fcc (100) surface, Au [110]. There is little doubt that it exists also in many other film/substrate combinations with $0.90 < \rho < 1.07$. However, it has not been recognized in the past LEED and RHEED studies. In LEED it is difficult to identify because it produces in its simplest form a c(2×2) pattern as the real space unit cell in figure 10(a) shows, in less well ordered stacking sequences more complicated patterns, usually with diffuse reflections and strong background because of the nonplanar crystal shape. In RHEED the pattern has erroneously been attributed to the fcc (110) orientation shown in figure 10(b). A reinterpretation [105] of the RHEED patterns of Ni on Au(100) and Fe(100) [111] clearly leads to the hcp ($11\bar{2}0$) orientation of figure 10(a). The c(2×2) RHEED pattern and the superlattice streaks off the main azimuths which are characteristic for the hcp structure were observed above 6 ML of pseudomorphic growth many years ago, but were not understood and therefore called 'reconstructed Ni' [112]. That their magnetic properties were found to be unusual is, in retrospective, understandable because the c-direction of the crystal is in plane in two orthogonal directions.

There are many other ferromagnetic film–nonmagnetic substrate combinations which fulfill the misfit criterion given above so that the hcp form of Ni and Fe can be expected also in other systems. Of course, it has to be kept in mind that the criterion is a necessary one but not a sufficient one. There is always the competition with pseudomorphic growth whenever $\rho \approx 1$. In the reverse case, nonferromagnetic film on ferromagnetic substrate the misfit criterion, of course, holds too. For example, Cu on Fe(100) ($\rho = 1.03$) is reported to be similar to Ni on Fe(100) [111] which means that it should also grow in hcp form after the initial pseudomorphic bcc layer [105]. The anisotropic local strain distribution in an hcp Cu layer possibly can influence the magnetic properties of an Fe layer grown on top of it. Thus a rich variety of magnetic phenomena can be expected in systems in which one of the layers has the hcp ($11\bar{2}0$) orientation or the fcc (110) orientation.

5. Growth on open and stepped surfaces

On open and stepped surfaces the substrate imposes its periodicity strongly on the initial film growth and intermixing is enhanced whenever it is driven by thermodynamics because of the lower kinetic barriers. The driving force to reach a dense interface packing makes the interface and consequently also the film less stable against agglomeration at elevated temperatures. Nevertheless it is possible to grow thin stable pseudomorphic layers and at low temperatures also thicker layers on open surfaces. Growth on stepped, that is, vicinal surfaces was studied initially in connection with the step-atom-induced in-plane anisotropies, more recently in connection with the growth of quasi-one-dimensional crystals. Only the latter work will be discussed.

5.1. Open surfaces

Growth on one open surface, the bcc (100) surface, has already been discussed in section 4.1. An even more open surface is the bcc (111) surface. Growth on it has been studied extensively (for references see [36] and [113–115]). Fe, Co and Ni, which have a large misfit with W, do not lead to W(111) faceting at elevated temperatures in contrast to many other metals with smaller misfit, but the layers are nevertheless thermally unstable. At room temperature Fe and Ni grow ML by ML up to 4 ML (in substrate atomic density units) before 3D growth sets in. In the case of Fe the first 2 ML are pseudomorphic; the next two are misfitting layers which have been attributed to slightly strained fcc Fe(111) layers. In Ni films the transition from pseudomorphic to misfitting layer occurs already during the growth of the second layer, resulting in a strained Ni(111) layer. Above 4 ML Ni faceted 3D Ni(111) crystals grow, relieving the strain in a manner similar to that observed in the growth of Ge on Si. Ni and Fe differ strongly in the thermal stability of thicker layers. Fe films agglomerate strongly, nearly spontaneously already below 400 K, the earlier the thicker the layer, while in Ni films the structural changes occur over a much larger temperature range. The difference may be due to spontaneous strain relaxation in Fe layer while in Ni layers the strain has already been relaxed during growth by faceting. An alternate explanation is interface alloying in Ni films—as indicated by LEED—which stabilizes the layer. More work is necessary to understand growth on bcc (111) surfaces.

While the bcc (111) surface is '2D open' the bcc (211), the fcc (110) and the hcp $(10\bar{1}0)$ and $(11\bar{2}0)$ surfaces are '1D open', that is they consist of troughs separated by ridges. The dense packing along the troughs and the larger trough–trough separation lead to a very anisotropic growth which has been observed in many STM studies on fcc (110) surfaces. Little use has been made up to now of this anisotropy in magnetic films and few growth studies have been made. An example is Ni on W(211) [11]. Ni forms at room temperature initially 3 ML (in units of the substrate atomic density). First the troughs are filled pseudomorphically, then the Ni chains in them are compressed to $6/7$ of the substrate atomic distance d_S. Next the ridges are occupied. With increasing filling of the ridges, the Ni–Ni distance decreases to 0.84 d_S but reverts back again to $6/7$ as soon as the third layer starts. The complete double layer may be considered as a somewhat wrinkled and distorted Ni(111) plane with the close-packed direction parallel to that of the substrate. Its atomic density is 4.2% larger than that of the Ni(111) plane in the bulk. Ni in excess of 3 ML grows in strongly anisotropic 3D (111)-oriented Ni crystals with the long dimension along the densely packed rows. Growth or annealing at high temperatures produces first a Ni_4W double layer. During the growth of a second double layer some Ni redistribution occurs so that the top layers have a higher Ni concentration. Excess Ni forms large 3D crystals. It is evident that the growth process is rather complicated as also seen in other films on fcc (110) surfaces by STM.

5.2. Stepped surfaces

Steps are generally preferred adsorption sites. Adsorption can occur either at the bottom or on the top of the step. As a rule of thumb, if the film material is less electronegative than the substrate the region with high electron density, that is the bottom site, is preferred, otherwise the top site. This is true both for Frank–van der Merwe and Volmer–Weber type systems. In the latter preferred nucleation has been used for decades to image otherwise invisible surface steps by 'decoration' with 3d Au or Pt crystallites [116] and for some time in the Frank–van der Merwe mode, for example to image steps on Mo(110) with PEEM by Cu decoration [117] (see also figure 5(a)). The pseudomorphic film grows from the step-by-step flow into stripes

with rather constant width if the steps are parallel and equally spaced. For magnetic studies straight, regular spaced steps are of interest. They can easily be obtained on vicinal surfaces on which step orientation and distance can be controlled by the misorientation. This method has been used to grow systems of straight Cu 'nanowires' on vicinal Mo(110) surfaces [118, 119], of straight monolayer Fe 'nanostripes' on vicinal W(110) surfaces [120] and of Fe double layer nanostripe arrays on the same surface [121]. The growth conditions for these linear 2D crystals are the same as those discussed for perfect monolayer growth. A counter-example to these Frank–van der Merwe type systems is Fe on vicinal Cu(111) [82, 83, 122, 123]. Fe has a higher surface energy and electronegativity than Cu and decorates the top of the steps in small 1–2 ML high crystals which grow together to nearly continuous rough wires as early as about 0.8 ML. This technique opens up many opportunities for magnetic studies on well controlled systems.

6. Film tailoring

Because of the intimate connection between structure and magnetic properties of thin films it is of fundamental importance to be able to produce and to reproduce the desired structure. What one usually would like to have are chemically pure layers with well defined thickness and strain, bounded by atomically flat unmixed surfaces/interfaces, sometimes with chosen geometry such as wire or strip arrays. The geometry can be controlled by substrate 'tailoring' as in section 5.2 or by producing a suitable substrate by thermal, chemical or electrochemical etching.

Strain is determined by the film–substrate combination and by the film thickness. With single-component substrates strain can only be varied in steps but alloy substrates, e.g. Au–Cu alloys, allow a continuous variation of strain. The goal of layers which are chemically pure or have a well defined composition with unmixed surfaces/interfaces is easily achieved by growing on substrates whose surface energy is larger than that of the film, at temperatures at which no interface alloying occurs. However, this recipe limits the number of substrate materials considerably and does not solve the problem of producing good sandwiches and superlattices because the high surface energy material has to be grown subsequently on the layer with lower surface energy γ. This favours Vollmer–Weber growth and/or intermixing and is counterproductive.

Therefore, different procedures have to be used in the two situations, low γ on high γ growth and high γ on low γ growth. In the first case the thermodynamically stable initial layers should be grown at high temperatures for optimum perfection, the subsequent layers at the highest temperature at which no agglomeration occurs. This maximizes diffusion, minimizes nucleation so that the kinetic roughening observed also in homoepitaxy is avoided. A three monolayer level growth front with large terraces can be achieved in this manner as illustrated in figure 6. Optimum high γ on low γ growth requires completely different conditions. In order to reach a continuous film as soon as possible after the nucleation of the double or multiple layer thick crystallites, the nucleation rate must be maximized. This is best done by growing on cooled substrates and/or at very high deposition rates. Pulsed laser deposition, which has been developed for the growth of high T_c superconductor films in order to transfer the chemical composition of the ablation target to the film, has been shown to be very effective also for the growth of films of interest here [124, 125]. Other methods are ion beam assisted and sputter deposition ([84] and references therein), more general methods for the creation of surface defects which act as nucleation sites, or simply high deposition rates at low temperatures [126]. Once the film is continuous and without substrate material on top so that the further growth is basically homoepitaxy the deposition conditions have to be changed to optimum

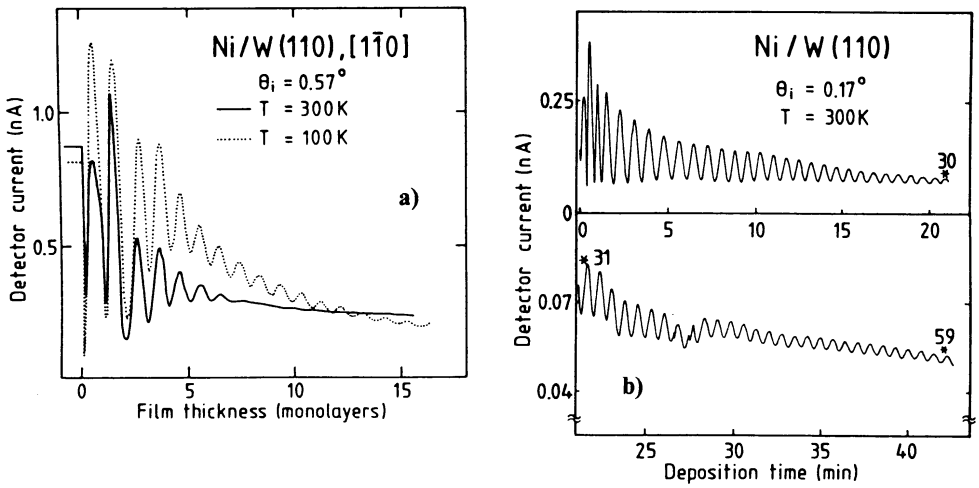

Figure 11. RHEED specular beam intensity oscillations during deposition of Ni on W(110) at a pressure of 8×10^{-11} mbar (a) and 1×10^{-8} mbar (b). Deposition rate 1.2 monolayers min^{-1} [15, 16].

homoepitaxy conditions—if this is possible without coalescence and surface segregation of the substrate material. Usually a compromise has to be made which depends upon the specific system.

The tendency to kinetic roughening can be reduced by surfactants which can be residual gas constituents [15, 16, 127, 128] or metals with low surface energy such as Pb [129–132]. Surfactants can act in at least two different ways: (i) they can reduce Ehrlich–Schwoebel barriers and thus enhance lateral growth of monolayer terraces while simultaneously reducing nucleation on top of them; (ii) they can block growth sites at steps, thus increasing the nucleation rate and suppressing the growth of large crystals. They stay on the surface which remains in general much flatter than in the absence of the surfactant. As an example figure 11 [15, 16] compares the influence of the pressure of the residual gas, which acts as a surfactant, with that of the temperature on the RHEED specular beam intensity oscillations during the growth of Ni films. The surfactant (figure 11(b)) is much more effective than cooling (figure 11(a)) in maintaining a reasonably flat surface. The surfactant Pb has also other beneficial effects. For example, in the growth of Cu on Co it suppresses twinning in the Cu layer which improves the continuity of the Cu layer so that Co deposited on top of it cannot couple directly ferromagnetically to the bottom layer [132]. In summary, the general rules for optimizing film growth are rather simple but the details may differ from system to system and require system-specific studies.

References

[1] 1999 *J. Magn. Magn. Mater.* **193** and earlier MRM conference proceedings
[2] Bauer E 1984 *The Chemical Physics of Solid Surfaces and Heterogeneous Catalysis* vol 3B, ed D D King and D P Woodruff (Amsterdam: Elsevier) p 1
Bauer E 1982 *Appl. Surf. Sci.* **11/12** 479
[3] Heinrich B and Bland J C A (eds) 1994 *Ultrathin Magnetic Structures* vol I (Berlin: Springer) ch 5
[4] King D A and Woodruff D P (eds) 1997 *The Chemical Physics of Solid Surfaces* vol 8 (Amsterdam: Elsevier)
[5] Bauer E 1994 *Rep. Prog. Phys.* **57** 895
[6] Schmidt Th, Heun S, Slezak J, Diaz J, Prince K C, Lilienkamp G and Bauer E 1998 *Surf. Rev. Lett.* **5** 1287

[7] Taylor N J 1966 *Surf.Sci.* **4** 161
[8] Moss R L L and Blott B H 1969 *Surf. Sci.* **17** 240
[9] Bauer E, Poppa H, Todd G and Bonczek F 1974 *J. Appl. Phys.* **45** 5164
[10] Bauer E and van der Merwe J H 1986 *Phys. Rev.* B **33** 3657
[11] Kolaczkiewicz J and Bauer E 1984 *Surf. Sci.* **144** 495
[12] Koziol C, Lilienkamp G and Bauer E 1987 *Appl. Phys. Lett.* **51** 901
[13] Berlowitz P J and Goodman D W 1987 *Surf. Sci.* **187** 463
[14] Kaemper K P, Schmidt W, Guentherodt G and Kuhlenbeck H 1988 *Phys. Rev.* B **38** 9451
[15] Lilienkamp G, Koziol C and Bauer E 1988 *Reflection High Energy Electron Diffraction and Reflection Imaging of Surfaces* ed P K Larsen and P J Dobson (New York: Plenum) p 489
[16] Bauer E, Jalochowski M, Koziol C and Lilienkamp G 1989 *Mater. Res. Soc. Symp. Proc.* vol 10 (Pittsburgh, PA: Materials Research Society) p 505
[17] Koziol C, Lilienkamp G and Bauer E 1990 *Phys. Rev.* B **41** 3364
[18] Li Y, Farle M and Baberschke K 1990 *Phys. Rev.* B **41** 9596
[19] Mingde X and Smith R J 1991 *J. Vac. Sci. Technol.* B **9** 1828
[20] Schmidthals C, Enders A, Sander D and Kirschner J 1998 *Surf. Sci.* **402–404** 636
[21] Sander D, Schmidthals C, Enders A and Kirschner J 1998 *Phys. Rev.* B **57** 1406
[22] Schmidthals C, Sander D, Enders A and Kirschner J 1998 *Surf. Sci.* **417** 361
[23] Tikhov M and Bauer E 1990 *Surf. Sci.* **232** 73
[24] van der Merwe J H and Bauer E 1994 *Phys. Rev.* B **49** 2127, 2137
[25] Hoeche H and Elmers H-J 1999 *J. Magn. Magn. Mater.* **191** 313
[26] Johnson B G, Berlowitz P J, Goodman D W and Bartholomew C H 1989 *Surf. Sci.* **217** 13
[27] Ociepa J G, Schultz P J, Griffiths K and Norton P R 1990 *Surf. Sci.* **225** 281
[28] Knoppe H and Bauer E 1993 *Phys. Rev.* B **48** 1794
[29] Fritsche H, Kohlhepp J and Gradmann U 1995 *Phys. Rev.* B **51** 15 933
[30] Bauer E 1997 *Handbook of Microscopy* ed S Amelinckx, D van Dyck, J van Landuyt and G van Tendeloo (Weinheim: VCH) p 751
[31] Duden T and Bauer E 1999 *Phys. Rev.* B **59** 474
[32] Wurm K 1994 *MS Thesis* TU Clausthal
[33] Duden T and Bauer E 1998 *J. Electron Microsc.* **47** 379
[34] Pinkvos H, Poppa H, Bauer E and Kim G-M 1993 *Magnetism and Structure in Systems of Reduced Dimension* ed R F C Farrow, B Dieny, M Donath, A Fert and B D Hermsmeier (New York: Plenum) p 25
[35] Gradmann U and Waller G 1982 *Surf. Sci.* **116** 539
[36] Gardiner T M 1983 *Thin Solid Films* **105** 213
[37] Przybylski M, Kaufmann I and Gradmann U 1989 *Phys. Rev.* B **40** 8631
[38] Gradmann U, Przybylski M, Elmers H-J and Liu G 1989 *Appl. Phys.* A **49** 563
[39] Berlowitz P J, He J W and Goodman D W 1990 *Surf. Sci.* **231** 315
[40] Bethge H, Heuer D, Jensen Ch, Reshoeft K and Koehler U 1995 *Surf. Sci.* **331–333** 878
[41] Sander D, Skomski R, Schmidthals C, Enders A and Kirschner J 1996 *Phys. Rev. Lett.* **77** 2566
[42] Bode M, Pascal R, Dreyer M and Wiesendanger R 1996 *Phys. Rev.* B **54** R8385
[43] Jensen C, Reshoeft K and Koehler U 1996 *Appl. Phys.* A **62** 217
[44] Bode M, Pascal R and Wiesendanger R 1997 *J. Vac. Sci. Technol.* A **15** 1285
[45] Sander D, Enders A, Schmidthals C, Reuter D and Kirschner J 1998 *J. Magn. Magn. Mater.* **177–181** 1299
[46] Kolaczkiewicz J and Bauer E, unpublished
[47] Malzbender J, Przybylski M, Giergiel J and Kirschner J 1998 *Surf. Sci.* **414** 187
[48] Albrecht M, Fritsche H and Gradmann U 1993 *Surf. Sci.* **294** 1
[49] Kamijo A 1993 *J. Magn. Magn. Mater.* **126** 59
Kamijo A 1996 *J. Magn. Magn. Mater.* **156** 137
[50] Knoppe H 1995 *PhD Thesis* TU Clausthal
[51] Sander D, Enders A, Schmidthals C, Reuter D and Kirschner J 1998 *Surf. Sci.* **402–404** 351
[52] Sander D, Skomski R, Enders A, Schmidthals C, Reuter D and Kirschner J 1998 *J. Phys. D: Appl. Phys.* **31** 663
[53] Bergholz R and Gradmann U 1984 *J. Magn. Magn. Mater.* **45** 55
[54] Stindtmann M, Farle M, Rahman T S, Benabid L and Baberschke K 1997 *Surf. Sci.* **381** 12
[55] Berlowitz P J, Houston J E, White J M and Goodman D W 1988 *Surf. Sci.* **205** 1
[56] Kolaczkiewicz J and Bauer E 1999 *Surf. Sci.* **423** 292
[57] Egawa C, Agura T and Iwasawa Y 1987 *Surf. Sci.* **185** L506
Egawa C, Agura T and Iwasawa Y 1987 *Surf. Sci.* **188** 563

[58] Liu C and Bader S D 1990 *Phys. Rev.* B **41** 553
[59] Andrieu S, Piecuch M and Bobo J F 1992 *Phys. Rev.* B **46** 4909
[60] Tian D, Li H, Jona F and Marcus P M 1991 *Solid State Commun.* **80** 783
[61] Ohresser P, Scheurer F, Carriere B, Deville J P and Dobroiu A 1996 *Surf. Sci.* **352–254** 567
Ohresser P, Scheurer F, Carriere B, Deville J P and Dobroiu A 1996 *Surf. Sci.* **364** 481
[62] Prieto J E, Rath Ch, Mueller S, Miranda R and Heinz K 1998 *Surf. Sci.* **401** 248
[63] Bulou H, Barbier A, Renaud G, Carriere B, Baudoing-Savois R and Deville J P 1997 *Surf. Sci.* **377–379** 90
[64] Voigtlaender B, Meyer G and Amer N M 1991 *Phys. Rev.* B **44** 10 354
[65] Wollschlaeger J and Amer N M 1992 *Surf. Sci.* **277** 1
[66] Toelkes C, Zeppenfeld P, Krzyzowski M, David R and Comsa G 1997 *Phys. Rev.* B **55** 13 932
[67] Padovani S, Molinas P, Scheurer F and Bucher J P 1998 *Appl. Phys.* A **66** 1199
[68] Padovani S, Scheurer F and Bucher J P 1999 *Europhys. Lett.* **45** 327
[69] Chambliss D D, Wilson R J and Chiang S 1991 *J. Vac. Sci. Technol.* **9** 933
Chambliss D D, Wilson R J and Chiang S 1991 *Phys. Rev. Lett.* **66** 1721
[70] Meyer J A, Baikie I D, Kopatzki E and Behm R J 1996 *Surf. Sci.* **365** L647
[71] Cullen W G and First P N 1999 *Surf. Sci.* **420** 53
[72] Stroscio J A, Pierce D T, Dragoset R A and First P N 1992 *J. Vac. Sci. Technol.* A **10** 1981
[73] Speckmann M, Oepen H P and Ibach H 1995 *Phys. Rev. Lett.* **75** 2035
[74] Toelkes Ch, Zeppenfeld P, Krzyzowski M, David R and Comsa G 1997 *Surf. Sci.* **394** 170
[75] Marsot N, Belkhou R, Scheurer F, Bartenlian B, Barrett N, Delaunay M A and Guillot C 1997 *Surf. Sci.* **377–379** 225
[76] Tyson W R and Miller W A 1977 *Surf. Sci.* **62** 267
[77] Gradmann U 1966 *Ann. Phys.* **17** 91
[78] Gradmann U 1974 *Appl. Phys.* **3** 161
[79] Persat N, Dinia A, Jay J P, Meny C and Panissod P 1996 *J. Magn. Magn. Mater.* **164** 37
[80] Rath Ch, Prieto J E, Mueller S, Miranda R and Heinz K 1997 *Phys. Rev.* B **55** 10 791
[81] Pedersen M O, Boenicke I A, Laegsgaard E, Stensgaard I, Ruban A, Norskov J K and Besenbacher F 1997 *Surf. Sci.* **387** 86
[82] Shen J, Skomski R, Klaua M, Jenniches H, Manoharan S S and Kirschner J 1997 *J. Appl. Phys.* **81** 3901
Shen J, Skomski R, Klaua M, Jenniches H, Manoharan S S and Kirschner J 1997 *Phys. Rev.* B **56** 2340–3
[83] Shen J, Klaua M, Ohresser P, Jenniches H, Barthel J, Mohan Ch V and Kirschner J 1997 *Phys. Rev.* B **56** 1134
[84] Wulfhekel W, Beckmann I, Rosenfeld G, Poelsema B and Comsa G 1998 *Surf. Sci.* **395** 168
[85] Speller S, Degroote S, Dekoster J, Langouche G, Ortega J E and Naermann A 1998 *Surf. Sci.* **405** L542
[86] van der Merwe J H and Bauer E 1989 *Phys. Rev.* B **39** 3632
[87] Tikhov M and Bauer E, figure 6 in [90]
[88] Duden T and Bauer E 1999 *Phys. Rev.* B **59** 468
[89] Duden T and Bauer E 1999 *J. Magn. Magn. Mater.* **191** 301
[90] Zhou X L, Yoon C and White J M 1988 *Surf. Sci.* **203** 53
[91] Jones T L and Venus D 1994 *Surf. Sci.* **302** 126
[92] Elmers H J and Hauschild J 1994 *Surf. Sci.* **320** 134
[93] Ociepa J and Bauer E, unpublished
[94] Johnson B G, Berlowitz P J, Goodman D W and Bartholomew C H 1989 *Surf. Sci.* **217** 113
[95] Wormeester H, Hueger E and Bauer E 1996 *Phys. Rev.* B **54** 17 108
[96] Bauer E and Duden T 1997 *J. Surf. Anal.* **3** 222
[97] Duden T 1996 *PhD Thesis* TU Clausthal
[98] Berlowitz P J and Goodman D W 1987 *Surf. Sci.* **187** 463
[99] Kellogg G L 1987 *Surf. Sci.* **192** L879
[100] Stroscio J A, Pierce D T and Dragoset R A 1993 *Phys. Rev. Lett.* **70** 3615
Stroscio J A, Pierce D T and Dragoset R A 1994 *J. Vac. Sci. Technol.* B **12** 1783
[101] Stroscio J A, Pierce D T, Unguris J and Celotta R J 1994 *J. Vac. Sci. Technol.* B **12** 1789
[102] Pierce D T, Stroscio J A, Unguris J and Celotta R J 1994 *Phys. Rev.* B **49** 14 564
[103] Wormeester H, Hueger E and Bauer E 1996 *Phys. Rev. Lett.* **77** 1540
[104] Wormeester H, Kiene M E, Hueger E and Bauer E 1997 *Surf. Sci.* **377–379** 988
[105] Hueger E, Wormeester H and Bauer E 1999 *Surf. Sci.* **438** 185
[106] Bruce L A and Jaeger H 1978 *Phil. Mag.* A **37** 337
Bruce L A and Jaeger H 1978 *Phil. Mag.* A **38** 223
Bruce L A and Jaeger H 1979 *Phil. Mag.* A **40** 97
[107] Donner W, Metocke N, Abromeit A and Zabel H 1993 *Phys. Rev.* B **48** 14 475

[108] Huang J C A, Liou Y, Liu H L and Wu Y J 1994 *J. Crystal Growth* **139** 363
[109] Wang C P, Wu S C, Jona F and Markus P M 1994 *Phys. Rev.* B **49** 17 391
[110] Oikawa S, Kanno T, Iwata S and Tsunashima S 1996 *J. Magn. Magn. Mater.* **156** 73
[111] Kamada Y and Matsui M 1997 *J. Phys. Soc. Japan* **66** 658
[112] Heinrich B, Purcell S T, Dutcher J R, Urquhart K B, Cochran J F and Arrott A S 1988 *Phys. Rev.* B **38** 12 879
[113] Guan J, Campbell R A and Madey T E 1995 *Surf. Sci.* **341** 311
[114] Madey T E, Guan J, Nien C H, Dong C-H, Tao H-S and Campbell R A 1996 *Surf. Rev. Lett.* **3** 1315
[115] Kolaczkiewicz J and Bauer E 1999 *Surf. Sci.* **420** 157
[116] Bassett G A 1958 *Phil. Mag.* **3** 1042
[117] Mundschau M, Bauer E and Swiech W 1988 *Surf. Sci.* **203** 412
[118] Jung T, Schlittler R, Gimzewski J K and Himpsel F J 1995 *Appl. Phys.* A **61** 467
[119] Petrovykh D Y, Himpsel F J and Jung T 1998 *Surf. Sci.* **407** 189 and references therein
[120] Hauschild J, Elmers H J and Gradmann U 1998 *Phys. Rev.* B **57** R677
[121] Hauschild J, Gradmann U and Elmers H J 1998 *Appl. Phys. Lett.* **72** 3211
[122] Brodde A, Dreps K, Binder J, Lunau Ch and Neddermeyer H 1993 *Phys. Rev.* B **47** 6609
[123] De la Figuera J, Huerta-Garnica M A, Prieto J E, Ocal C and Miranda R 1995 *Appl. Phys. Lett.* **69** 1006
[124] Shen J, Jenniches H, Mohan Ch V, Barthel J, Klaua M, Ohresser P and Kirschner J 1998 *Europhys. Lett.* **43** 349
[125] Shen J, Ohresser P, Moran Ch V, Klaua M, Barthel J and Kirschner J 1998 *Phys. Rev. Lett.* **80** 1980
[126] Buergler D E, Schmidt C M, Schaller D M, Meisinger F, Hofer R and Guentherodt H-J 1997 *Phys. Rev.* B **56** 4149
[127] Steigerwald D A, Jacob I and Egelhoff W F Jr 1988 *Surf. Sci.* **202** 472
[128] Egelhoff W F Jr and Steigerwald D A 1989 *J. Vac. Sci. Technol.* A **7** 2167
[129] Egelhoff W F Jr, Chen P J, Powell C J, Stiles M D, Michael R D, Lin C-L, Sivertsen J M, Judy J H, Takano K and Berkowitz A E 1996 *J. Appl. Phys.* **80** 5183
[130] Chopra H D, Hockey B J, Chen P J, Egelhoff W F Jr, Wuttig M, de Miguel J J and Miranda R 1997 *Phys. Rev.* B **55** 8390
[131] Camarero J, de Miguel J J, Graf T, Miranda R, Kuch W, Zharnikov M, Dittschar A, Schneider C M and Kirschner J 1998 *Surf. Sci.* **402–404** 346
[132] Camarero J, Spendeler L, Schmidt G, Heinz K, de Miguel J J and Miranda R 1994 *Phys. Rev. Lett.* **73** 2448